

# Optical FBG-T Based Fault Detection Technique for EV Induction Machines

Wenping Cao<sup>1</sup>, Belema P. Alalibo<sup>2</sup>, Bing Ji<sup>3</sup>, Xiangping Chen<sup>4</sup> and Cungang Hu<sup>1</sup>

<sup>1</sup>School of Electrical Engineering and Automation, Anhui University, Hefei, China, 230601

<sup>2</sup> College of Engineering & Physical Sciences, Aston University, Birmingham, UK, B4 7ET

<sup>3</sup>Department of Engineering, University of Leicester, Leicester, UK, LE1 7RH

<sup>4</sup>College of Engineering, Guizhou University, Guiyang, China, 550025

*Abstract*—Electric vehicles (EV) represent a key technology to achieve a low-carbon transportation objective, whilst induction motors are one of the promising topologies. The reliability of these machines is crucial to minimize the downtime, cost and unwanted human lives. Although several techniques are utilized in the condition monitoring and fault detection of electrical machines, there is still no single technique that provides an all-round solution to fault detection in these machines and thus hybrid techniques are used widely. This paper presents a novel non-invasive optical fiber technique in condition monitoring of induction machines and in the process detecting inter-turn short circuit faults. Owing to optical fiber's immunity to magnetic flux, a composite FBG-T sensor formed by bonding a giant magnetostrictive transducer, Terfenol-D, onto a fiber Bragg grating is utilized to sense machines' stray flux as a signature to determine the internal winding condition of the machines. A tri-axial auto datalogging flux meter was used to obtain the stray magnetic flux and test results obtained via LabView were analyzed in MatLab. Experimental and numerical results agree with each other and how that the FBG-T sensor accurately and reliably detected the short-circuit faults. Bragg shifts observed under short-circuit faults were in 100s of picometre range under various operating frequencies compared to the mid-10s of picometre obtained under healthy machine condition. These provide much promise for future EVs.

## 1. INTRODUCTION

MANKIND must adapt to a more sustainable way of living to avoid the catastrophic impacts of climate change; the electric vehicles (EVs) provide a solution to reduce carbon emissions related to road transportation. Of all the industrial motors in use globally, induction motors are the most common type [1]. Transitioning to full mode electric transport – be it on land, air or sea; more renewable power generation and even more sustainable industrial practices would mean that electric machines are expected to undoubtedly play an important role. Thus, the reliability and continuous availability of these electric machines is pivotal to industry. The reality however is that electric machines are susceptible to unexpected breakdown due to the often harsh and highly stressed environments [2] under which they are operated in order to provide the goods and services humans need. Many electric machines run 24/7 all year round across various industrial plants with minimal downtime for scheduled or routine maintenance. Unexpected machine failures and consequent downtimes do have serious operational and financial adverse impacts including repair or replacement costs, stopping production processes with



consequent economic losses, likely impact on the company's reputation, and customer dissatisfaction. Real time online condition monitoring of these machines is crucial now more than ever, as reliability of these machines is a sine qua non to boosting end user confidence in transiting to the dream world of net zero carbon emissions. Various condition monitoring and fault detection techniques are currently available each having its own limitations [3]; however, there exists no single signature or technique that is capable of diagnosing all possible machine failures [4]. Best industrial practice optimally utilizes a multi-monitoring approach where two or more of available techniques are simultaneously deployed for comprehensive real time condition monitoring and fault detection in electric machines. Given the crucial role of these machines both in the present and in future, and the vast and rapidly increasing number of usage of these machines globally, there will never be a superfluous number of condition monitoring and fault detection techniques. Therefore, increasing the pool of available machine condition monitoring options is rather an urgent and welcome development.

Optical fiber sensors continue to find applications in various fields owing to their high reliability, low cost and zero electromagnetic interference in addition to other numerous advantages. Fiber Bragg gratings (FBG) appear to be the most commonly used optical fiber sensor in recent times with most recent applications in various fields. The use of FBG sensors for electric machine condition monitoring have been invasive hitherto; with FBG sensors usually mostly installed within stator slots or circumferentially around stator windings. Optical fibers are generally very brittle and highly susceptible to breakage. With invasive techniques, sensor replacement would require downtimes and temporarily disconnecting the machines which would have economic and social consequences depending on the service being disrupted. Hitherto, there is no known FBG sensor that measures magnetic field in a non-intrusive manner utilizing external stray flux to determine an electric machine condition as well as detect faults. Although the external stray flux is typically attenuated by the machine cast frame, its small magnitude can be adequately detected by optics given that the order of magnitude of the broadband laser used for such sensors, are typically in the nanometer (nm) range. FBGs on its own are immune to electromagnetic field hence a transducer is needed to convert the stray magnetic field into strain before it can be optically detected. Terfenol-D, a giant magnetostrictive alloy is used to achieve this purpose where the FBG is bonded onto the alloy using cyanoacrylate adhesive which transfers the strain movement from the alloy to the FBG and then subsequently observed as a wavelength shift known as Bragg shift on an optical spectrum analyzer (OSA).

## 2. PRINCIPLE OF FBG SENSING

Light refraction occurs because air has a different refractive index from the medium through which the light now travels. In other words, due to the difference in atomic particulate composition of different materials, the speed at which light travels through different mediums is not the same resulting in the bending phenomenon. Although the frequency of the light wave does not change, its wavelength changes [5] and the relationships between its speed in air ( $c$ ), its speed in a different medium ( $v$ ), the refractive index of the medium ( $n$ ), its wavelength ( $\lambda$ ) and its frequency ( $f$ ) are given by:

$$c = f\lambda \quad (1)$$

$$n = \frac{c}{v} \quad (2)$$

According to Snell's law of refraction, the ratio of the refractive indices of the materials ( $n_1$  and  $n_2$ ) at the boundary surface equals the ratio of the sine of the angles of incidence ( $\theta_1$ ) and transmission ( $\theta_2$ ). He also relates the refractive indices to the wavelengths in each medium  $\lambda_1$  and  $\lambda_2$  as follows:

$$\frac{n_1}{n_2} = \frac{\lambda_2}{\lambda_1} = \frac{\sin\theta_2}{\sin\theta_1} \quad (3)$$

Light reflection follows that the angle of incidence must equal the angle of refraction i.e.  $\theta_1 = \theta_2$ . The reflection of light at the interface (boundary) between two different medium is also known as Fresnel's reflection effect. Investigations in physics do show that the refracted angle tends to get smaller than the incident angle when light is travelling from a fast medium to a slow one (for example, air to water). Conversely, for light travel from water to air, for example, the incident angle tends to get larger but it

cannot exceed  $90^\circ$  while remaining in the new medium. Hence this incident angle constraint suggests that the largest incident angle for refraction occurs when  $n_2 < n_1$ . However, beyond a certain incident angle known as critical angle,  $\theta_c$ , there will be no refraction at all and the light wave will be totally reflected away from the new medium through which the light was intended to travel provided  $n_2 < n_1$  still exists. This is called total internal reflection which is the phenomenon used in optical fibers. In a typical optical fiber silica cable, its core with a higher refractive index,  $n_1$  is surrounded by a cladding whose refractive index,  $n_2$  is only about 1% lower than that of the core in order to satisfy the condition for total internal reflection. For example, the core could have  $n_1 \approx 1.4475$  and the cladding  $n_2 = 1.444$  and provided the fiber cable is not excessively bent; the light will just bounce around in the cable with minimal loss [5].

Uniform FBG is the standard FBG in which the gratings have equal and evenly spaced distance called the period between them. They are fabricated usually using a phase mask technique [6] to expose a short length of photosensitive fiber to a periodic distribution of light such that the fiber's refractive index is permanently varied in accordance with the exposure of the light intensity as shown in Fig. 1.

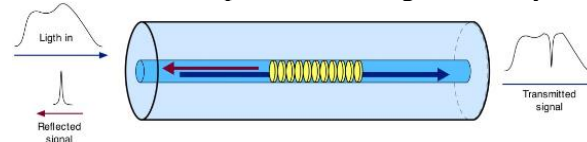


Fig. 1: FBG - Fibre cladding with evenly spaced gratings within its core [7]

When the light is guided along the fiber core comes in contact with the inscription of the gratings, it is weakly reflected by each grating plane by Fresnel effect [8]; and the reflected light from each grating plane then recombines with other reflections in the backward direction in either a constructive or destructive interference pattern depending on if the wavelength of the incoming light satisfies Bragg's law given by:

$$2d \sin \theta = n \lambda \quad (4)$$

With the light's incident angle  $\theta = 90^\circ$  and  $d$ , the distance between peaks of the interference pattern, then for vacuum with refractive index,  $n=1$ ;  $\lambda=2d$  is the approximate wavelength of the reflection peak which means the fiber reflects part of the incoming spectrum [8]. For silica material used to make optical fiber, the distance travelled by light,  $d$  is affected by the material's refractive index,  $n$ , thus equation (4) can be adapted for silica as:

$$2n_{eff} \Lambda = \lambda_B \quad (5)$$

where  $\lambda_B$  is the Bragg wavelength,  $n_{eff}$  is the effective refractive index of the fiber and  $\Lambda$  is the periodicity of the grating. It is possible to change the Bragg wavelength also known as 'Bragg Shift' by either varying the fiber's effective refractive index or the grating periodicity or both. This is the fundamental principle of the FBG sensing. By designing the proper interface, desired measurement can be made to impose some external force or disturbance on the grating (such as temperature, vibration, pressure, and displacement) which will result in a Bragg shift proportional to the external force applied, as shown in Fig. 2.

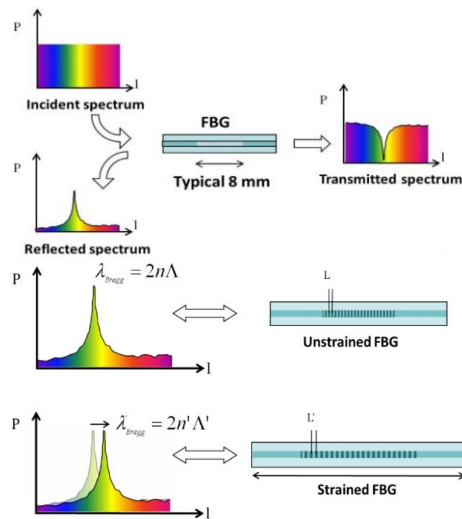


Fig. 2: a) Light spectrum – incident, transmitted and reflected; b): Bragg shift concept [9]

### 3. EXPERIMENTAL METHOD

Since optical fiber is immune to magnetic flux, if FBG were to be used for sensing magnetic field, it will require a transducer to convert the magnetic flux into one of the strains to be able to cause Bragg shifts. Terfenol-D is used in this research to achieve the transduction of magnetic flux into strain which is then impressed on the FBG via an adhesive acting as a transfer medium. Prior to carrying out experiments, the effects of the number of bonding points on metal-surface mount FBG sensors was investigated and reported in [10] which takes account of the impact of the adhesive used.

The complete set up used for this work is as shown in Fig. 3. The FBG-T test rig set up for both healthy and short circuit inter-turn fault conditions. Each of the test induction motors is used to drive a DC motor with the FBG-T sensor transversely positioned relative to the rotor shaft at the drive end (DE) of the induction motor. Stray magnetic flux data was acquired using an auto datalogger gaussmeter - HHG1394 - manufactured by Omega Engineering UK. The HHG1394 comes with proprietary software and a tri-axial sensing functionality which makes it suitable for low and extremely low frequency magnetic fields independent of measurement angle. The FBG-T sensor is then connected to a dual-functional broadband light source and optical spectrum analyzer (OSA) which is serially connected to a PC via National Instrument GPIB cable. This is to allow the use of LabView software to collect and store numerical spectral data that can be retrieved and analyzed in MatLab.



Fig. 3: Complete experimental test rig for FBG-T stray flux sensing

The motor was driven by a variable frequency drive (VFD). Each machine was run at similar frequency range between 5 – 30Hz with 5Hz interval initially for two hours without the auto data logger and then repeated for four hours with the auto data logger, after which the motor is then turned off each time. Prior to running the healthy motor, it was disassembled and observed to confirm its healthy state before reassembly. For short circuit inter-turn conditions, strands of copper windings were used to bridge turns within the motor as shown in Fig. 4.



Fig.4: Healthy and Inter-turn fault conditions prior to assembly

#### 4. RESULTS AND DISCUSSION

In order to carry out any experiments, it was imperative to determine the optimal location where the sensor should be positioned as well as to calibrate the sensor to determine its sensitivity.

##### 4.1 Optimal FBG-T Location

Two major factors were taken into consideration in positioning the FBG-T: proximity to the main air gap flux and sensor surface area exposed to the external flux. The closest part of the machine to the main air gap flux is the flange coupling at the drive end (DE) of the machine. Hence, this was one of the positions considered.

Three possible axes to position the sensor at the DE are: transverse (perpendicular to rotor shaft), inclined (intermediate between parallel and perpendicular to rotor shaft) or axial or longitudinal (parallel to rotor shaft). The second option was very quickly dis-carded because magnetic fields are well known to be either at their maximum field strength or zero depending on whether the flux lines are cutting across a surface either perpendicularly or in parallel to the surface respectively. Transverse and longitudinal positions were later empirically tested to identify the optimal sensor position.

The variation of observable stray flux with frequency for both transverse and axial sensor positions showed that more flux will cut across the sensor when placed in the transverse position at the drive end of the machine compared to the axial position (Fig. 5). Although this has been attributed to reduced surface area of the flux-attenuating and corrugated yoke, one can argue that the transverse position is closer to the source of the magnetic flux which is in the air gap within the machine. This is because the air gap is between the rotor and the stator whose windings are wrapped internally close to the flanges of the machine. Based on the optical spectral response only, there was no observable difference in terms of sensor position; instead there were evidence that the FBG-T sensor was indeed sensing the stray magnetic flux present. From both the behavioral characteristics and observable magnetic flux density viewpoints, the transverse position became the experimental choice and thus was utilized throughout the rest of the investigation.

##### 4.2 FBG-T Flux Calibration

For the magnetic field source, an openly-wound 4V DC motor whose windings were exposed was used with a DC power supply unit to provide the need current for different magnetic field strengths. A tri-axial auto data logger magnetic flux meter was used to measure and record the stray magnetic flux density for each applied current. Different amount of currents was applied generate magnetic field of different strengths measured by the auto data logging flux meter.

The optical spectra showed an increase in the Bragg shift with current given that the magnetic flux as measured by the auto data logger gauss meter also increased with current as expected (Fig. 6). Time varying plots of Bragg shifts showed a steady increase in the Bragg shifts with time until the maximum Bragg shift was attained. The rate at which the Bragg shifts occurred for each current value appeared to be faster than the rate observed for earlier tests performed with alternating stray flux. This could be

attributed to the impact the sinusoidal nature of the ac flux has on the magnetic dipole of the Terfenol-D particles causing them to move faster to a new equilibrium state when magnetic flux is present. Fig. 6 confirms the sensitivity of the FBG-T sensor which was  $19.3810\text{pm}/\mu\text{T}$  with room temperature reasonably constant with a recorded maximum change of about  $0.13^\circ\text{C}$ .

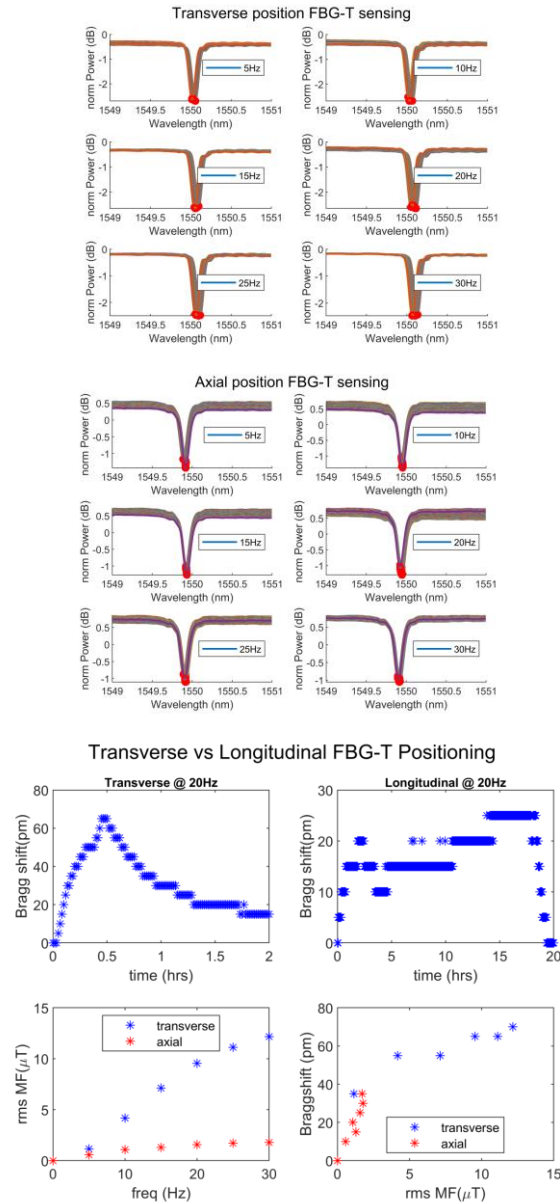
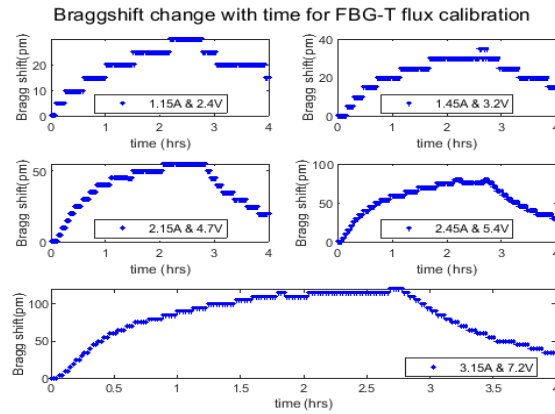


Fig. 5: Comparison between FBG-T sensed parameters when in transverse and axial sensor positions

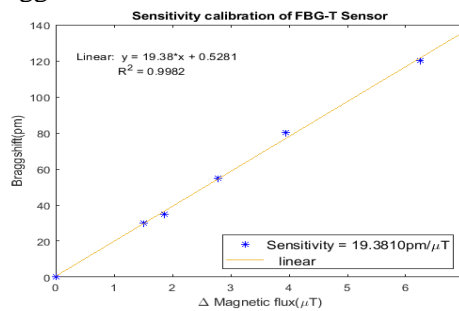
#### 4.3 FBG-T Short Circuit Inter-Turn Fault Detection

Observations confirmed significant temperature rise in the case of the short circuit inter-turn fault and a dramatic increase in Bragg shift accompanied by a set of rather near-normal magnetic flux readings for frequency between 5Hz and 15Hz. By 20Hz it was observed that both the temperature and magnetic flux had reduced unexpectedly developing some curiosity as to why. The unexpected reduction in temperature and magnetic field strength necessitated the need to confirm of the copper conductor strands were still in place, and the inter-turn fault condition had not been compromised. After the motor was disassembled it was observed that part of the stator winding had burnt out which was the reason for the reduced temperature and magnetic flux as a smaller number of conductors were carrying current.

Therefore, the investigation was halted at this stage as the FBG-T sensor has proved to be very reliable in detecting such serious fault condition non-intrusively using stray flux. A repeat test was later performed with a smaller number of strands to attempt to avoid burning the stator windings on an identical machine, and also substantiate this crucial observation.



b) Braggshift variation with time at various currents



d) Sensitivity of the FBG-T sensor

Fig. 6: Magnetic flux FBG-T sensor calibration results

In order to detect the aberration from the healthy motor condition, data from both conditions were analyzed in Table 1. Bragg shifts observed with increase in frequency and in turn magnetic flux clearly showed a stark path between both motor conditions due to the severity of the inter-turn fault.

Whilst Bragg shifts were in the tens of picometer (pm) for the healthy condition, they were in the hundreds of picometer for the short circuit condition (Fig. 7) which is a succinct feature fundamental to the use of FBG-T sensor in fault detection.

TABLE 1: Comparison Of Braggshifts Changes With Temperature At Different Frequencies

Frequency (Hz)	Healthy Braggshifts (pm)	Inter-turn Braggshifts (pm)	Healthy ΔTemp. (°C)	Inter-turn ΔTemp. (°C)
5	30	290	0.7615	3.3538
10	50	530	0.5600	4.2700
15	45	645	1.4692	5.5692

The disparity between the intensity of the stray magnetic flux was not large as only a few turns of extra copper conductor strands were added to emulate the fault condition. Fig. 8 shows a slight increase in the magnetic flux for the faulty condition compared to the healthy state due to a slightly higher current producing the magnetic flux. However, the temperature difference was very significant (Fig. 8)

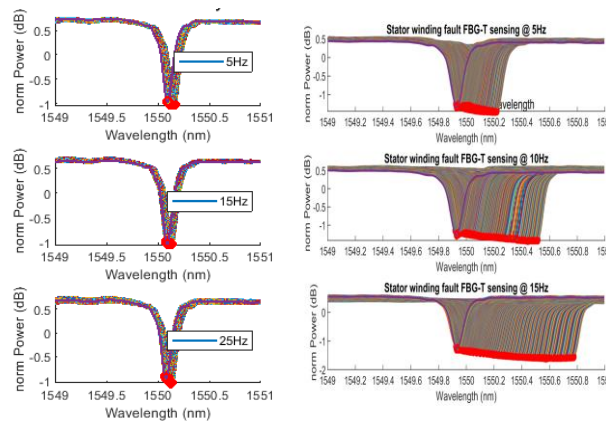


Fig. 7: Optical spectral response under healthy and inter-turn fault conditions

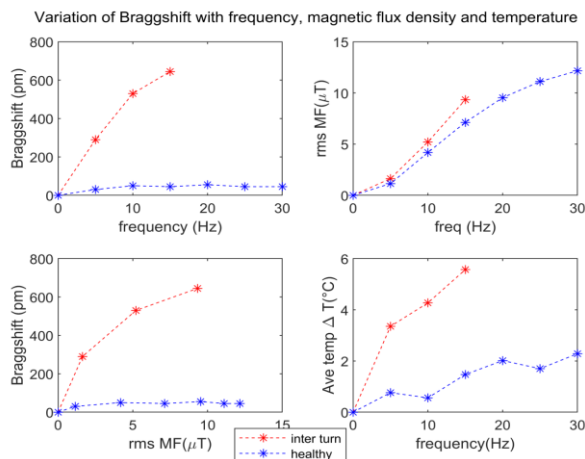


Fig. 8: Variation of frequency with Bragg shifts, external magnetic flux density and temperature under more short circuit faults

The noticeable large wavelength shifts are largely due to the over-temperature caused by the increased  $I^2R$  losses as a result of the inter-turn short circuit fault. These large Bragg shifts required several hours to return to their initial wavelength as shown in Fig. 9, clearly justifying the presence of a magnetic field and its effect on the Bragg shifts. It thus confirms that the Bragg shifts are due to both the magnetic flux and the over-temperature caused by the inter-turn short circuit condition as the result was consistent at all three frequencies. Another key observation is that regardless of machine condition, the FBG-T sensor exhibited reversible magnetization as shown in Fig. 9. This is because of the small amplitude of the stray flux which is insufficient in causing a permanent change of state of the magnetic dipoles of the Terfenol-D alloy. Thus, whenever the magnetic flux is removed, the magnetic dipoles lose their magnetization and attempt to return to their initial state of equilibrium.

##### 5. REPRODUCIBILITY TEST: FBG-T INTER-TURN FAULT DETECTION WITH AUTO DATA LOGGER

Earlier a similar test was performed but with more copper conductor strands which resulted in burnt stator windings following the over-riding of the built-in overcurrent protection in the VFD. In order to avoid a repeat of such damage, less number of conductor strands was used to allow for testing over the entire test frequency range which was not achievable previously due to the damage to the motor. Motor was run from 5-30Hz with 5Hz interval as before but this time for the duration of four (4) hours and turned off for 16 hours per frequency to allow for sensor reset. Test results show the new induction motor with inter-turn fault emulated using less number of copper strands.

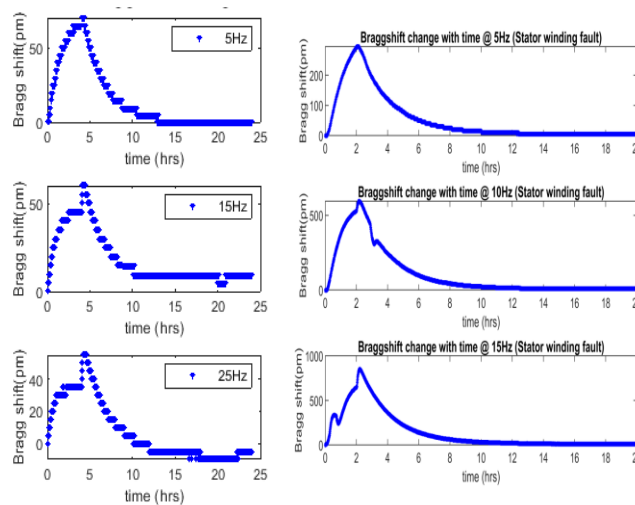


Fig. 9: Time varying braggshift response of FBG-T sensor under healthy and inter-turn fault conditions

With a longer duration of operation, there was consistency in the behavior of the FBG-T sensor with respect to Bragg shifts. The shift in wavelengths appear to rise and plateau within the four hours, and once the machine was turned off, a clear descent path back to the initial wavelength due to reversible magnetization as earlier explained. The FBG-T behavior described was observed when the motor was run at the different frequencies. Another key observation was that throughout the short circuit condition test, the FBG-T was observed to show less hysteresis when returning to its initial wavelength. This may be due to the spectral content of the stray magnetic flux as the other external factor (ambient temperature) which could affect the sensor was reasonably constant with minimal variation. It is worthy of mention that while this reduced hysteresis may be desired, it does not affect the use of the FBG-T sensor for fault detection because the underpinning principle of FBG sensing in general depends of the magnitude of Bragg shifts.

Table 2 shows that the order of magnitude of Bragg shifts observed during inter-turn fault condition are in hundreds of picometre which is clearly very high. These large Bragg shifts were succinct in the optical spectra at different frequencies where the wavelength shifts increased with frequency. In theory it would be easy to associate the large Bragg shifts to the increase in magnetic flux density or temperature or a combination of both factors. From Table 2 there is a direct but non-proportional increase in Bragg shifts with magnetic flux density as well as with maximum temperature change as frequency increased which agrees with theory. However, for such a large magnitude of Bragg shift when compared to corresponding values of magnetic flux density and temperature changes in healthy machine condition and during sensor calibration, it is difficult to convincingly suggest that only the amplitudes of these two measurands (flux and temperature) are responsible. With the aid of the auto datalogger, the magnetic flux obtained will be subjected to spectral analysis to further analyze its contents.

### 5.1 Healthy versus Inter-turn Conditions

Compared to the healthy condition where Bragg shifts are barely just over 50pm irrespective of the frequency at which the motor is run; under inter-turn fault condition the Bragg shifts are well over 100pm even up to over 400pm. In fact, the Bragg shifts directly responded to the change in the motor frequency. This was identical to the earlier observed when there were more number of shorted turns that burnt the stator winding initially. Though the experiment was halted after the motor damage incident, the trajectory for the both the healthy and the inter-turn conditions in the two tests were identical and clear in the accuracy of the FBG-T sensor to detect the short circuit faulty condition. The magnetic flux densities measured in both tests were of similar range as well and when compared with the frequency range showed an increase in amplitude as motor frequency increased.

Considering the magnitude of the stray flux is in micro-tesla range, the difference in flux densities

between successive frequencies was less than  $5\mu\text{T}$  which is really small to cause such large Bragg shifts. When compared to the healthy condition, the magnitude of the flux density of both healthy and inter-turn fault conditions were in the same range with increasing difference between corresponding values as frequency increased. For example, at 10Hz the difference in magnetic flux density between healthy and inter-turn conditions was about  $0.145\mu\text{T}$  whereas at 20Hz and 30Hz the same difference was about  $3.13\mu\text{T}$  and  $4.16\mu\text{T}$  respectively. Same observation was made previously with a greater number of shorted turns and less operating time. With respect to the maximum temperature change observed in both reduced and higher number of turns the results were identical. As expected, due to the short circuit the maximum observed temperature change increased as frequency increased as the motor is made to do more work. Due to the difference in the number of turn in both tests, the temperature changes were slightly different. For instance, at 15Hz a maximum temperature change of  $3.953^\circ\text{C}$  was observed for this test with a smaller number of turns compared to  $5.5692^\circ\text{C}$  for the previous test with a greater number of turns. This is expected due to more  $I^2R$  losses in the previous test. When compared to the healthy machine state, identical results in both tests showed that the maximum temperature change was always less than  $1.7^\circ\text{C}$  across all the individual motor frequency of operation which is still lower than the lowest temperature change observed under short circuit condition for both tests. Another observation was that unlike in healthy state where there was no evidence of a direct relationship between temperature variation across operating frequencies; there was a clear and direct proportionality for the short circuit condition. As the motor frequency increased, the temperature also increased due to the additional short circuit  $I^2R$  losses which increase with loading on a motor.

## 6. CONCLUSIONS

A novel condition monitoring technique which utilizes FBG-T sensor to detect inter-turn faults in EV induction machines has been investigated. FBG-T sensing reliability and accuracy has been tested under healthy and short circuit machine conditions. From analytical and experimental results, it is evident that: 1) the FBG-T sensor can reliably and accurately monitor the condition of the machines; 2) the proposed method can unambiguously detect the short circuit faults with succinctly large Bragg shifts observable via the pre-analysed sensor's optical spectra; 3) Bragg shifts vary with time, frequency and temperature from the post-analysed plots and are thus used for detection and reasoning. However, the magnitude of the flux densities obtained is not enormously large to cause such significant Bragg shifts especially for the short circuit conditions. In the future work, a fast Fourier transform (FFT) method will be used in the data analytics for those acquired by the auto datalogger, and a study on harmonic contents of the stray flux from the FBG-T sensors.

## REFERENCES

- [1] Schneider Electric, "Monitoring Induction Motors for Energy Savings (Part 2)," PowerLogic Solut., vol. 8, no. 2, 2006.
- [2] P J Zhang, Y Du, T G Habetler, and B Lu, "A Survey of Condition Monitoring and Protection Methods for Medium-Voltage Induction Motors," *Ieee Trans. Ind. Appl.*, vol. 47, no. 1, pp. 34–46, 2011.
- [3] Israel Zamudio-Ramirez, Roque A. Alfredo Osornio-Rios, Jose Alfonso Antonino-Daviu, Hubert Razik, and Rene de Jesus Romero-Troncoso, "Magnetic Flux Analysis for the Condition Monitoring of Electric Machines: A Review," *IEEE Trans. Ind. Informatics*, 2021.
- [4] Maria J. Picazo-Rodenas, Jose Antonino-Daviu, Vicente Climente-Alarcon, Rafael Royo-Pastor, and Ariel Mota-Villar, "Combination of Noninvasive Approaches for General Assessment of Induction Motors," *IEEE Trans. Ind. Appl.*, vol. 51, no. 3, pp. 2172–2180, May 2015.
- [5] Matthew Schwartz, "Refraction and Reflection," Lecture note. [Online]. Available: <https://scholar.harvard.edu/files/schwartz/files/lecture15-refraction.pdf>. [Accessed: 10-Oct-2021].
- [6] National Instruments, "Fundamentals of Fiber Bragg Grating (FBG) Optical Sensing - National Instruments," 2016. [Online]. Available: <http://www.ni.com/white-paper/11821/en/>.

[Accessed: 27-Nov-2017].

- [7] Carlos A. J. Gouveia, Jose M., and Pedro A.S., “Refractometric Optical Fiber Platforms for Label Free Sensing,” in *Current Developments in Optical Fiber Technology*, InTech, 2013.
- [8] Marcelo M., Regina C. S. B. Allil, Bessie A., and Fbio V. B. de Nazar, “A Guide to Fiber Bragg Grating Sensors,” in *Current Trends in Short- and Long-period Fiber Gratings*, InTech, 2013.
- [9] Hongli Li, Gang Xu, Xin Gui, Lei Liang, and Zhengying Li, “An FBG Displacement Sensor in Deformation Monitoring of Subway Floating Slab,” *IEEE Sens. J.*, 2021.
- [10] Belema P. Alalibo, Wenping Cao, Adenowo Gbadebo, Lassi Aarniovuori, and Kewei Cai, “Investigation of the effect of bonding points on metal surface-mounted FBG sensors for electric machines,” *Prog. Electromagn. Res. C*, 2019.